

Vortex Formation in Spin–Orbit Coupled Spin-1 Bose Condensates with Magnetic Field

QIANG ZHAO*

Department of Applied Physics, North China University of Science and Technology, Tangshan 063210, China

Received: 30.10.2023 & Accepted: 04.03.2024

Doi: [10.12693/APhysPolA.145.227](https://doi.org/10.12693/APhysPolA.145.227)

*e-mail: zhaoqiangac2004@sina.com

In this article, we study the vortex formation in spin-1 spin–orbit coupling rotating Bose–Einstein condensates. Numerical results are obtained by solving the spinor Gross–Pitaevskii equation. We mainly focus on the influences of external magnetic fields on vortex structures and dynamics properties. With the increase in magnetic field strength, the populations of magnetic components $j = \pm 1$ reach the identical value. For the density profile, the three components present identical density structures, and the size of condensates is nearly the same. In addition, some related physical quantities, such as the time taken for the arrival of a steady population and root-mean-square size, kinetic energy, and total angular momentum, are calculated. The results show that these quantities decrease as the magnetic field strength increases. Moreover, we also investigate the time evolution of angular momentum. It is seen that the dynamic behavior of the magnetic components $j = \pm 1$ is exactly consistent, and the total angular momentum reduces in the presence of the strong magnetic field. This reflects the fact that the introduction of the strong magnetic field makes it difficult to rotate the condensate, and thus, it is disadvantageous for generating more vortices.

topics: vortex, spin–orbit coupled, magnetic field, spinor condensates

1. Introduction

Rotating Bose–Einstein condensates (BECs) provide a highly controllable experimental platform for the investigation of quantized vortices [1, 2]. Physically, a vortex is a typical topological defect with a quantized winding number of the phase and plays an important role in superconductors [3], helium superfluids [4], and astrophysics [5]. Following the generation of quantized vortices, much attention has been paid to the formation of vortex lattices [6], hidden vortices [7], vortex glass state [8], and vortex in the Berezinskii–Kosterlitz–Thouless phase transition [9], and so on. For a review of the studies of vortex in a rotating BEC, see [10] and references therein.

The first experimental realization of spin–orbit coupling (SOC) by the NIST group [11] opens an active area of research in condensed matter physics. Generally speaking, SOC originates from the interaction between the intrinsic spin of an electron and the magnetic field induced by its motion. Experimentally, SOC can lead to a variety of novel topological natures, such as insulators [12], superconductors [13], and semimetals [14]. In addition, SOC also offers a peculiar ground for studying different contexts, including half-quantum vortex [15], stripe phase [16], and elementary excitations [17]. In addition, bright and

dark solitons [18], solitonic structures [19] in single and multi-component BEC [20], and mixed Rashba–Dresselhaus couplings [20] have been widely studied in the past few years.

Recently, there has been a growing interest in the influences of external magnetic fields on BECs. The dynamical instability induced by the magnetic field is studied in anti-ferromagnetic BECs [21], where four types of instability are displayed. In [22], the authors investigate the critical behavior of the magnetic-field-induced phase transition via magnetization and specific heat measurements. The BECs of magnons are likely to be in magnets because magnons are bosonic quasiparticles of a magnetically ordered system. The interaction between magnons that affects the magnon BEC in a two-sublattice antiferromagnet without and with an external magnetic field is expounded [23]. Furthermore, the interaction effect on the ground state of BEC of charged bosons is analyzed from the viewpoint of spontaneous symmetry breaking. It has been found that the ground state of such a BEC is a quantized vortex with large circulation [24].

Our objective in this paper is to study the effects of external magnetic fields on vortex dynamics. Numerical results show that the vortex structure and vortex formation process are greatly affected by magnetic fields. This article is organized as follows. In Sect. 2, we formulate the theoretical

model of spin-1 spin-orbit coupled rotating BECs with homogeneous magnetic field, and the details of the numerical method are presented. In Sect. 3, the influences of the magnetic field on the dynamics properties are discussed. It is shown that the populations of magnetic components $j = \pm 1$ reach the same value as the magnetic field strength increases. The three components display identical density profiles, and the size of the condensates is nearly the same. Additionally, the physical quantities, such as the time taken for the arrival of a steady population and root-mean-square (rms) size, kinetic energy, and total angular momentum, decrease with an increase in the magnetic field strength. Furthermore, the time evolution of angular momentum for the magnetic components $j = \pm 1$ is exactly consistent, and the total angular momentum reduces in the presence of the strong magnetic field. These results reflect the fact that the strong magnetic field is disadvantageous for creating more vortices. Finally, we present a brief summary in Sect. 4.

2. Theoretical model

We take into account a three-component BEC of atom mass m in a crossed optical dipole trap. The dynamics of the BEC in the presence of external magnetic field B is governed by minimizing the three-dimensional (3D) energy functional $E = E_1 + E_2$ [25, 26]. The single-particle energy E_1 is given by

$$E_1 = \int d\mathbf{r} \Psi^\dagger \left[-\frac{\hbar^2}{2m} \nabla^2 + V_{3D}(\mathbf{r}) + v_{\text{soc}} - \Omega L_z + g_F \mu_B \mathbf{B} \cdot \mathbf{F} \right] \Psi, \quad (1)$$

where Ψ_j ($j=1,0,-1$) are the component wave functions, ∇^2 is the three-dimensional Laplacian, and t is the time. The trap potential $V_{3D} = \frac{1}{2}[m\omega_\perp^2(x^2+y^2) + \omega_z^2 z^2]$, where ω_\perp and ω_z are trap frequencies along the radial and axial direction, respectively. Now, $\mathbf{F} = (F_x, F_y, F_z)$ is the spin-1 matrices, and spin density $\mathbf{S} = \sum_{i,j} \psi_i^* \mathbf{F}_{ij} \psi_j$, $S_\pm = (S_x \pm iS_y)/\sqrt{2}$. The term ΩL_z appears in a system rotating about the z -axis at a rotation frequency Ω , where $L_z = -i\hbar(x\partial_y - y\partial_x)$. The Bohr magneton is denoted as μ_B and the Landé g -factor as g_F . In (1), $v_{\text{soc}} = -i\hbar\kappa(F_x\partial_y - F_y\partial_x)$ is Rashba-type SOC with strength κ . The s -wave contact interaction energy is written as

$$E_2 = \frac{1}{2} \int d\mathbf{r} [c_0 \rho(\mathbf{r}) + c_2 \mathbf{S}^2(\mathbf{r})], \quad (2)$$

where $c_0 = \frac{4\pi\hbar^2}{3m}(a_0+2a_2)$ and $c_2 = \frac{4\pi\hbar^2}{3m}(a_2-a_0)$ are the interaction between atoms, with a_0 and a_2 being two-body s -wave scattering lengths for total spin 0 and 2, respectively. The total atomic density $\rho(\mathbf{r}) = \sum_j |\Psi_j(\mathbf{r})|^2$ satisfies $\int \rho(\mathbf{r}) d\mathbf{r} = N$, where N is the total number of atoms.

In this paper, we focus on the dynamic properties of a quasi-two-dimensional (quasi-2D) condensate. In this case, the trap frequencies in the axial direction are much greater than in the radial direction. Therefore, the dynamics of the BEC in the axial direction ground state $\phi(z)$ is frozen. The wave function can be factorized as $\Psi(\mathbf{r}) = \phi(z)\psi(x, y) = \frac{1}{(2\pi d_z)^{1/4}} \exp(-\frac{z^2}{4d_z^2})\psi(x, y)$, where $\psi(x, y)$ is the 2D wave function in the x - y plane and $d_z = \sqrt{\omega_\perp/\omega_z}$. By using the variational procedure $(i-\gamma)\hbar\partial\Psi_i = \delta E/\delta\Psi_i^*$, one can obtain the coupled 2D Gross-Pitaevskii (GP) equation for the radial wave function ψ_j

$$\begin{aligned} (i-\gamma)\frac{\partial\psi_1}{\partial t} &= \left[-\frac{1}{2}\Delta^2 + V_{2D} + \beta_n n + \beta_s(n_1+n_0-n_{-1}) - \Omega L_z \right] \psi_1 + \beta_s \psi_{-1}^* \phi_0^2 + B\psi_0 + \lambda(i\partial_y + \partial_x)\psi_0, \\ (i-\gamma)\frac{\partial\psi_0}{\partial t} &= \left[-\frac{1}{2}\Delta^2 + V_{2D} + \beta_n n + \beta_s(n_1+n_{-1}) - \Omega L_z \right] \psi_0 + 2\beta_s \psi_1 \psi_{-1} \psi_0^* + B(\psi_1 + \psi_{-1}) \\ &\quad + \lambda \left[(i\partial_y - \partial_x)\psi_1 + (i\partial_y + \partial_x)\psi_{-1} \right], \\ (i-\gamma)\frac{\partial\psi_{-1}}{\partial t} &= \left[-\frac{1}{2}\Delta^2 + V_{2D} + \beta_n n + \beta_s(n_0+n_{-1}-n_1) - \Omega L_z \right] \psi_{-1} + \beta_s \psi_1^* \psi_0^2 + B\psi_0 + \lambda(i\partial_y - \partial_x)\psi_0, \end{aligned} \quad (3)$$

where $\Delta^2 = \partial_{xx} + \partial_{yy}$, $V_{2D} = \frac{1}{2}(x^2+y^2)$. In (3), $n_j = |\psi_j|^2$ is the density of the j -th component, and the population of the hyperfine state is $N_j = \int d\mathbf{r} n_j$. The total density $n = \sum_j n_j$, and the wave function is normalized to the total number of

atoms $N = \sum_j N_j$. The spin-independent and spin-dependent interactions are $\beta_n = \frac{2N(a_0+2a_2)}{3} \sqrt{\frac{\pi\omega_z m}{\hbar}}$ and $\beta_s = \frac{2N(a_0-a_2)}{3} \sqrt{\frac{\pi\omega_z m}{\hbar}}$. In turn, λ is the SOC strength. Note that the γ parameter accounts for the dissipation, and it relaxes the condensate

into the stationary pattern and is assumed to be $\gamma = 0.03$. The assumption is reasonable and is utilized in the pioneering work [27]. Here, the unit of length, time, energy, angular momentum, rotation frequency, and SOC strength for dimensionless calculation are $\sqrt{\hbar/(m\omega_\perp)}$, $1/\omega_\perp$, $\hbar\omega_\perp$, \hbar , ω_\perp , and $\sqrt{\hbar\omega_\perp/m}$, respectively.

Numerically, we initially prepare the stable ground state wave function by solving equation (3) using the imaginary time evolution approach [28] without rotating, dissipation, and external magnetic field. Namely, the initial states of the BEC are in the $F = 1$ hyperfine ground state. The dynamic evolution is performed by the split operator method [29]. The specific steps are as follows

$$\begin{aligned} (i - \gamma)\partial_t\psi_j &= \left(-\frac{1}{2}\partial_{xx} - i\Omega y\partial_x\right)\psi_j, \\ (i - \gamma)\partial_t\psi_j &= H_A\psi_j, \\ (i - \gamma)\partial_t\psi_j &= H_B\psi_j, \\ (i - \gamma)\partial_t\psi_j &= \left(-\frac{1}{2}\partial_{yy} + i\Omega x\partial_y\right)\psi_j, \end{aligned} \quad (4)$$

where H_A and H_B are 3×3 matrix operators, their expressions defined as

$$H_A = \lambda \begin{pmatrix} 0 & i\partial_y + \partial_x & 0 \\ i\partial_y - \partial_x & 0 & i\partial_y + \partial_x \\ 0 & i\partial_y - \partial_x & 0 \end{pmatrix} \quad (5)$$

and

$$H_B = \begin{pmatrix} V_{2D} + \beta_n n + \beta_s(n_1 + n_0 - n_{-1}) & \beta_s\psi_0\psi_{-1}^* + B & 0 \\ \beta_s\psi_0^*\psi_{-1} + B & V_{2D} + \beta_n n + \beta_s(n_1 + n_{-1}) & \beta_s\psi_0^*\psi_1 + B \\ 0 & \beta_s\psi_0\psi_1^* + B & V_{2D} + \beta_n n + \beta_s(n_0 + n_{-1} - n_1) \end{pmatrix}. \quad (6)$$

It is important to emphasize that the norm of the wave function does not conserve in the time evolution of (3). This is due to the influence of dissipation. To address this issue, we treat the chemical potential as time-dependent to ensure the normalization of the wave function. Technically, the kinetic energy term is calculated by the pseudospectral method [30], and the matrices H_A and H_B are solved using the numerical diagonalization method [31]. The space and time steps in our calculation are 0.125 and 0.001, respectively. Such a choice of step lies in that it can quickly converge to the ground state, and the split operator method for dynamic is much easier to implement.

3. Results and discussion

The richness of the present system lies in the large number of free parameters, which include the strength of the contact interactions, SOC, rotation frequency, and external magnetic field. In the following, we consider $N = 6000$ condensated ^{87}Rb atoms. The s -wave scattering length $a_0 = 101.8a_B$ and $a_2 = 100.4a_B$, where a_B is Bohr radius. The trap frequencies for the radial and axial direction are $\omega_{\perp,z} = 2\pi \times (10, 100)$ Hz. Under this condition, the dimensionless contact interactions are $\beta_n = 1488.25$ and $\beta_s = -6.89$. To highlight the effect of the external magnetic field, we fix β_n, β_s and set $\lambda = 1.0$, $\Omega = 0.6\omega_\perp$, with the implicit assumption that the dynamics properties are dominated by the external magnetic fields.

We first discuss the populations of magnetic components for different magnetic field strengths. We focus on the time scale of the population oscillation.

Figure 1a shows the time evolution of the population at a weak magnetic field $B = 0.01$ mG. The black, red, and blue lines represent $j = 1, 0$, and -1 , respectively. These lines fast oscillate from $t = 0$ to a certain time and finally reach a fixed value. We define this certain time as t_a . Namely, t_a is the time needed to reach a steady population. It is clear that coherent oscillations are observed. Coherent oscillations mean that the transfer of population persists over time and does not become chaotic even for large times. In addition, the fixed value is distinct for three components, and t_a is about 32. With an increase in magnetic field $B = 0.05$ mG in Fig. 1b, it is found that the components $j = \pm 1$ fluctuate around the almost same value, and t_a decreases to 16.3. This result reflects that increasing magnetic field strength enables reaching the steady state faster. Moreover, this point is further verified in the case of $B = 0.1$ mG and $B = 0.5$ mG, which is displayed in Fig. 1c and d, respectively. It is obvious that t_a significantly decreases, and the populations for components $j = \pm 1$ are identical. In Fig. 2a, we plot t_a as a function of magnetic field strength.

The magnitude of kinetic energy E_k is a significant physical quantity in the dynamics process. In earlier work [32], the variation of kinetic energy in spin-1 antiferromagnetic ^{23}Na condensate is shown with zero magnetic field. In addition, the rotating external magnetic field is applied to the Bose gas of magnetic atoms. Here, we investigate this issue for different magnetic field strengths. Figure 3 displays E_k as a function of time t at various magnetic field strengths. It is remarkable that E_k slowly increases and then saturates for $B = 0.01, 0.05, 0.1$ mG. However, as magnetic field strength is increased to $B = 0.5$ mG, E_k spikes to a peak and then

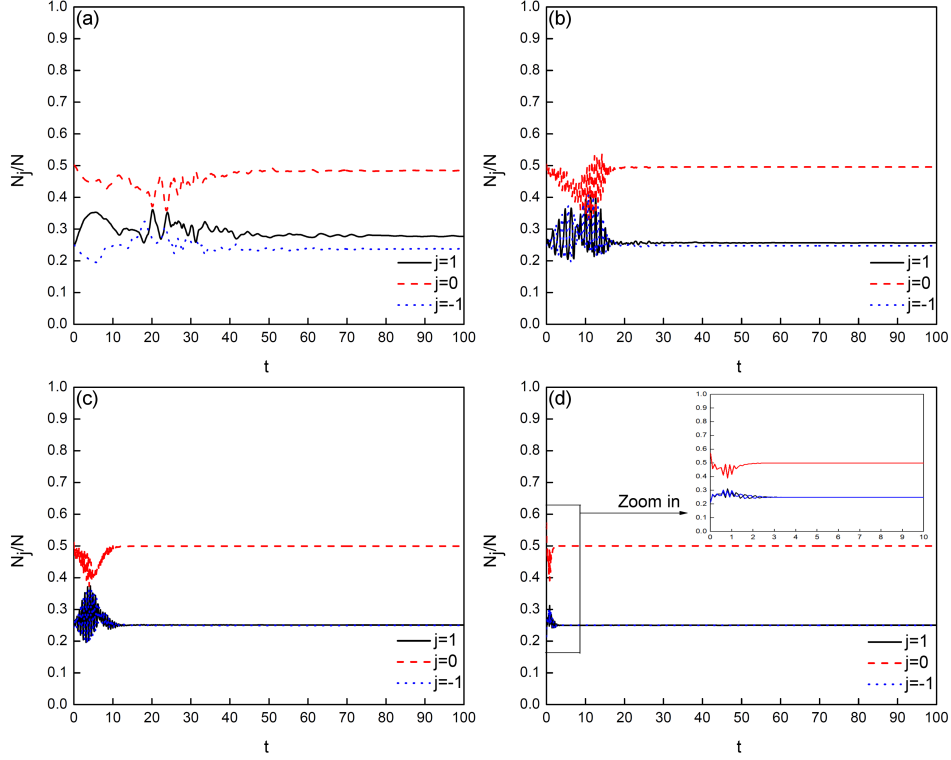


Fig. 1. Populations of atom clouds N_j/N as a function of time t . The magnetic fields are (a) $B = 0.01$ mG, (b) $B = 0.05$ mG, (c) $B = 0.1$ mG, and (d) $B = 0.5$ mG. The black, red, and blue lines represent $j = 1, 0, -1$ components, respectively. Simulation parameters: $\beta_n = 1488.25$, $\beta_s = -6.89$, $\lambda = 1.0$, and $\Omega = 0.6\omega_\perp$. The units of time and strength of SOC are ω_\perp^{-1} and $\sqrt{\hbar\omega_\perp}/m$, respectively.

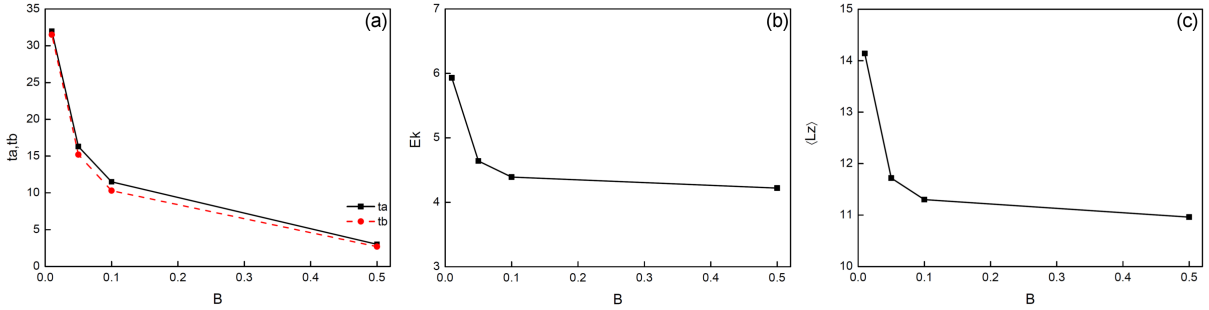


Fig. 2. Effects of external magnetic field on some physical quantities; (a) the time needed to reach a steady population t_a and rms size t_b ; (b) kinetic energy E_k ; and (c) total angular momentum $\langle L_z \rangle$. From left to right, the four points correspond to magnetic field strength $B = 0.01$ mG, 0.05 mG, 0.1 mG, and 0.5 mG, respectively. Simulation parameters: $\beta_n = 1488.25$, $\beta_s = -6.89$, $\lambda = 1.0$, and $\Omega = 0.6\omega_\perp$. The units of time, energy, angular momentum, and strength of SOC are ω_\perp^{-1} , $\hbar\omega_\perp$, \hbar and $\sqrt{\hbar\omega_\perp}/m$, respectively.

decreases sharply to a steady level. Moreover, it is worth mentioning that a key feature of our numerical results for the kinetic energy in the steady state is that it decreases with the increase in magnetic field strength, as displayed in Fig. 2b. The physical mechanism can be explained as follows. Our result shows that the time spent for the formation of steady-state vortices decreases with the increase in magnetic field strength. As for the dynamic evolution process, the steady-state vortices imply that the system arrives in an ordered state. From

the point of classical mechanics, when the system is in an ordered state, the movement of the atom decelerates and thus leads to smaller kinetic energy. In addition, the same time for the kinetic energy to settle down at different external magnetic fields indicates that the magnetic field is irrespective of this time scale.

To get a better insight into the role of the external magnetic field, we analyze the spatial structure of different magnetic components. Figure 4 shows the time development of density profiles at $B = 0.01$ mG.

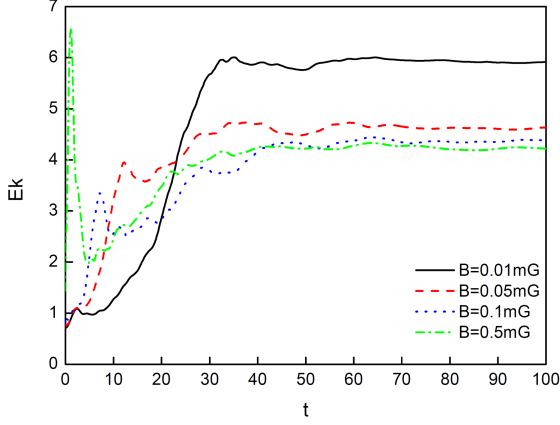


Fig. 3. Time evolution of the kinetic energy E_k as a function of t . The black, red, blue, and green lines represent the case of $B = 0.01$ mG, 0.05 mG, 0.1 mG, and 0.5 mG, respectively. Simulation parameters: $\beta_n = 1488.25$, $\beta_s = -6.89$, $\lambda = 1.0$, and $\Omega = 0.6\omega_\perp$. The units of time, energy, and strength of SOC are ω_\perp^{-1} , $\hbar\omega_\perp$, and $\sqrt{\hbar\omega_\perp/m}$, respectively.

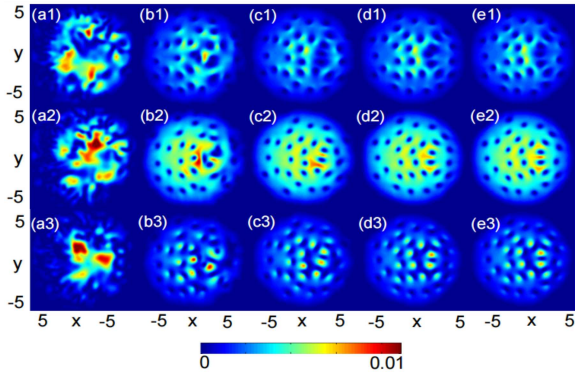


Fig. 4. Density profiles for the spin-1 BEC of ^{87}Rb atom. From top to bottom, the rows represent n_1 , n_0 , and n_{-1} . From left to right, the columns represent (a) $t = 20$, (b) $t = 40$, (c) $t = 60$, (d) $t = 80$, (e) $t = 100$. Simulation parameters: $\beta_n = 1488.25$, $\beta_s = -6.89$, $\lambda = 1.0$, $\Omega = 0.6\omega_\perp$, and $B = 0.01$ mG. The units of time, length, and strength of SOC are ω_\perp^{-1} , $\sqrt{\hbar/(m\omega_\perp)}$ and $\sqrt{\hbar\omega_\perp/m}$, respectively..

From top to bottom, the rows represent n_1 , n_0 , and n_{-1} , respectively. We take the components $j = 0$ to expound the change in vortex structure, and the evolution process of component $j = \pm 1$ is similar to the case of $j = 0$. At $t = 20$, the surface of BECs becomes unstable, and ripples are induced. Then, these ripples gradually develop into vortices and achieve a stable configuration at time $t = 100$. As a result, a circular vortex necklace forms. The characteristic of a vortex necklace is that vortices link up with each other in a ring. Moreover, we note that this configuration is also observed in anti-ferromagnetic SOC spin-1 BECs [33] and rotating binary BECs [34].

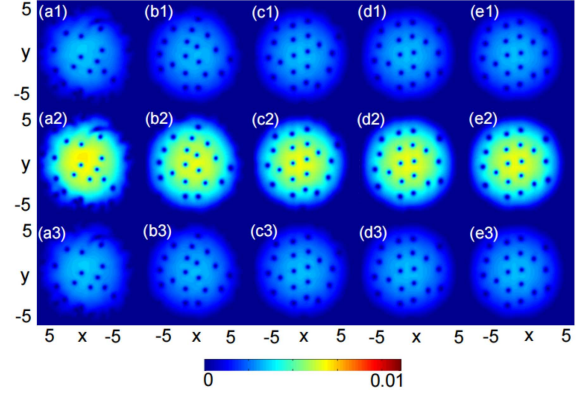


Fig. 5. Density profiles for the spin-1 BEC of ^{87}Rb atom. From top to bottom, the rows represent n_1 , n_0 , and n_{-1} . From left to right, the columns represent (a) $t = 20$, (b) $t = 40$, (c) $t = 60$, (d) $t = 80$, (e) $t = 100$. Simulation parameters: $\beta_n = 1488.25$, $\beta_s = -6.89$, $\lambda = 1.0$, $\Omega = 0.6$, and $B = 0.5$ mG. The units of time, length, and strength of SOC are ω_\perp^{-1} , $\sqrt{\hbar/(m\omega_\perp)}$ and $\sqrt{\hbar\omega_\perp/m}$, respectively.

When the magnetic field strength is increased, the difference occurs in density profiles. Figure 5 displays the time development with $B = 0.5$ mG. At $t = 20$, the space structure of the three components and the size of the condensate are nearly the same. Despite small structural adjustments, such features are kept until $t = 100$. Note that the size of the three components is different in the case of $B = 0.01$ mG. To more precisely examine the size change of condensates, we plot the time evolution of rms size $R_{\text{rms}} = \sqrt{\langle x^2 \rangle + \langle y^2 \rangle}$ [35] in units of $\sqrt{\hbar/m\omega_\perp}$, $\langle A \rangle = \iint dx dy \psi^* A \psi$, which is shown in Fig. 6. The black, red, and blue lines represent components $j=1, 0$, and -1 , respectively. Similarly, we find that these lines fast oscillate from $t = 0$ to a certain time and then remain almost unchanged. We define t_b as the time needed to reach the steady rms size, and it significantly reduces as the magnetic field strength increases. Moreover, the dependence of t_b on magnetic field strength B is shown in Fig. 2a. It is obvious that t_b is approximately equal to t_a .

In rotating BECs, the vortex formation can be quantitatively described by angular momentum $\langle L_z \rangle_j$, which is defined as

$$\langle L_z \rangle_j = -i \iint dx dy \psi_j^* (x\partial_y - y\partial_x) \psi_j. \quad (7)$$

Figure 7 shows the time evolution of $\langle L_z \rangle_j$ per atom with respect to time t for magnetic field strength. Overall, $\langle L_z \rangle_j$ gradually increases with some oscillations and then attains a steady value. This means that a stable vortex lattice is formed. In this process, the evolution behavior is different for $B = 0.01$ mG, and $\langle L_z \rangle_j$ presents three values. As a consequence, the atom density in three components presents three structures. With the increase

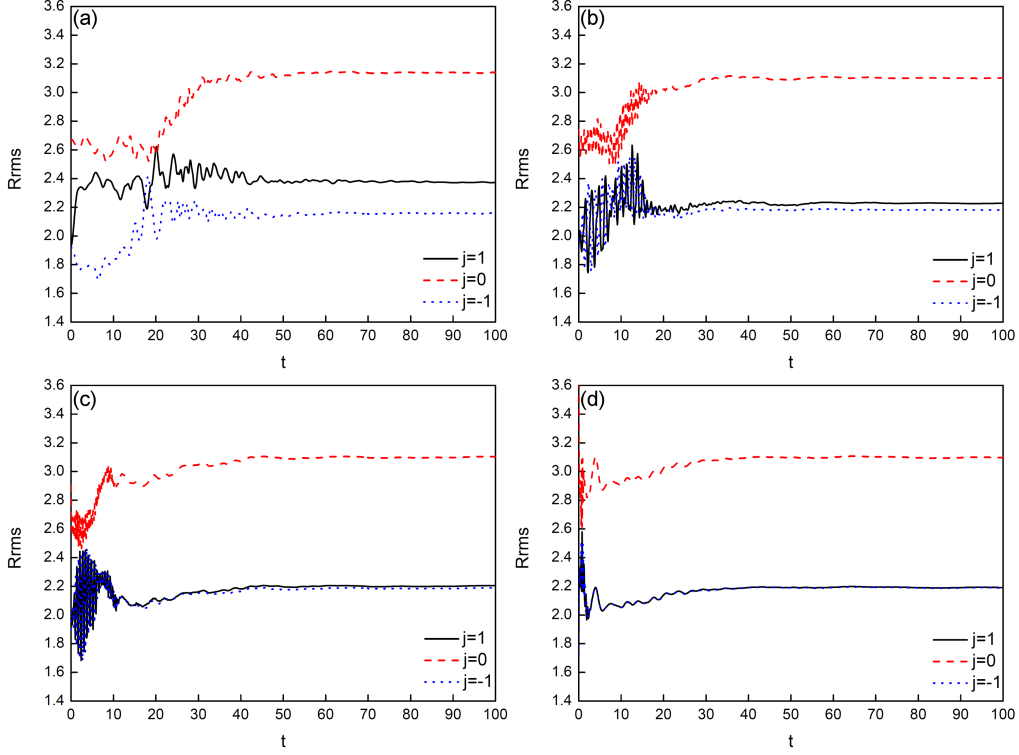


Fig. 6. Numerical result for rms size for the component wave functions ψ_j as a function of time t . The external magnetic fields are (a) $B = 0.01$ mG, (b) $B = 0.05$ mG, (c) $B = 0.1$ mG, and (d) $B = 0.5$ mG. Simulation parameters: $\beta_n = 1488.25$, $\beta_s = -6.89$, $\lambda = 1.0$, and $\Omega = 0.6\omega_\perp$. The units of time, rms size, and strength of SOC are ω_\perp^{-1} , $\sqrt{\hbar/(m\omega_\perp)}$, and $\sqrt{\hbar\omega_\perp/m}$, respectively.

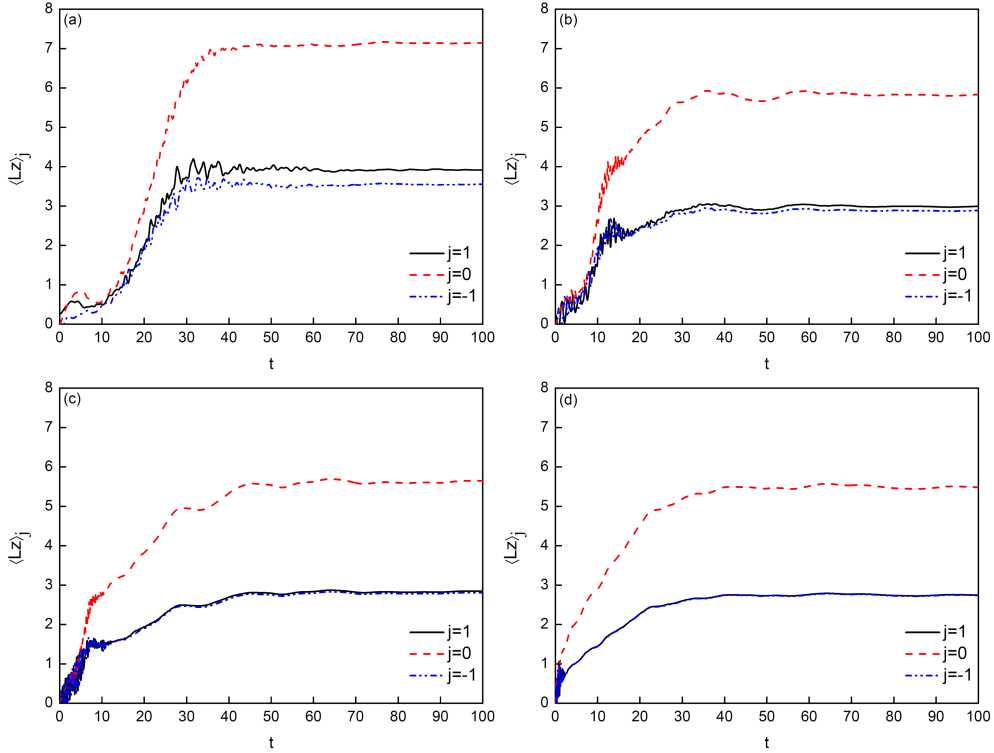


Fig. 7. Time evolution of the angular momentum $\langle L_z \rangle_j$ as a function of time t . The black, red, and blue lines represent $\langle L_z \rangle_1$, $\langle L_z \rangle_0$, and $\langle L_z \rangle_{-1}$, respectively. The magnetic fields are (a) $B = 0.01$ mG, (b) $B = 0.05$ mG, (c) $B = 0.1$ mG, and (d) $B = 0.5$ mG. Simulation parameters: $\beta_n = 1488.25$, $\beta_s = -6.89$, $\lambda = 1.0$, and $\Omega = 0.6\omega_\perp$. The units of time, angular momentum, and strength of SOC are ω_\perp^{-1} , \hbar , and $\sqrt{\hbar\omega_\perp/m}$, respectively.

in magnetic field strength $B = 0.5$ mG, however, the behavior is exactly coincident for components $j = \pm 1$ and thus $\langle L_z \rangle_1 = \langle L_z \rangle_{-1}$. In this case, the same vortex structure is seen in $j = \pm 1$. In addition, we also note that $\langle L_z \rangle_0 > \langle L_z \rangle_1$. The difference may be attributed to the inhomogeneous density. Furthermore, we calculate the total angular momentum $\langle L_z \rangle = \langle L_z \rangle_1 + \langle L_z \rangle_0 + \langle L_z \rangle_{-1}$, which is shown in Fig. 2c. It is evident that increasing magnetic field strength leads to a decrease in the total angular momentum. This fact suggests that a strong magnetic field is unfavorable for creating more vortices.

Before conclusion, we would like to point out that the results presented above can be further extended to other situations. In this article, we consider the external magnetic field to be homogeneous. Recently, the gradient magnetic field has been widely discussed, and many novel properties have been found [36–38]. It is estimated that the physical picture may be different from the results in this paper. In addition, it is known that vortices in BECs can be generated via an artificial magnetic field [39, 40]. In this case, instead of following the axis of rotation, the vortex structures are modulated by the geometry of the magnetic field profiles. Therefore, the tunable creation of an artificial magnetic field is the other feasible route to investigating the vortex formation process.

4. Conclusions

In conclusion, we study the vortex formation in spin-1 SOC rotating BECs with homogeneous magnetic fields. Our results show that the vortex dynamics are greatly influenced by magnetic field. With an increase in magnetic field strength, the populations of magnetic components $j = \pm 1$ go from two independent values to approximately the same value. In addition, the time needed to reach the steady state dramatically decreases. In addition, the amount of kinetic energy also displays a similar variation trend. As for the density profile, we find that the three components possess identical patterns, and the size of the condensates is nearly the same. The quantitative calculation shows that the time taken for the arrival of steady rms size significantly reduces. Finally, we analyze the time evolution of angular momentum. It is indicated that the behavior for the components $j = \pm 1$ is exactly coincident, and the total angular momentum decreases, which implies that a strong magnetic field is disadvantageous for generating more vortices.

Acknowledgments

This work is supported by the Innovation Fund of North China University of Science and Technology (Grant No. X2022266).

References

- [1] M.R. Matthews, B.P. Anderson, P.C. Haljan, D.S. Hall, C.E. Wieman, E.A. Cornell, *Phys. Rev. Lett.* **83**, 2498 (1999).
- [2] K.W. Madison, F. Chevy, W. Wohlleben, J. Dalibard, *Phys. Rev. Lett.* **84**, 806 (2000).
- [3] *Superconductivity*, Ed. R.D. Parks, Dekker, New York 1969.
- [4] R.J. Donnelly, *Quantized Vortices in Helium II*, Cambridge University Press, Cambridge 1991.
- [5] M. Kobayashi, M. Nitta, *Phys. Rev. C* **107**, 045801 (2023).
- [6] P. Engels, I. Coddington, P.C. Haljan, E.A. Cornell, *Phys. Rev. Lett.* **89**, 100403 (2002).
- [7] T. Mithun, K. Porsezian, B. Dey, *Phys. Rev. A* **89**, 053625 (2014).
- [8] B. Rosenstein, D. Li, *Rev. Mod. Phys.* **82**, 109 (2010).
- [9] Z. Hadzibabic, P. Krüger, M. Cheneau, B. Battelier, J. Dalibard, *Nature* **441**, 1118 (2006).
- [10] A.L. Fetter, *Rev. Mod. Phys.* **81**, 647 (2009).
- [11] Y.J. Lin, K. Jiménez-García, I.B. Spielman, *Nature* **471**, 83 (2011).
- [12] M.Z. Hasan, C.L. Kane, *Rev. Mod. Phys.* **82**, 3045 (2010).
- [13] X.L. Qi, S.C. Zhang, *Rev. Mod. Phys.* **83**, 1057 (2011).
- [14] X.G. Wan, A.M. Turner, A. Vishwanath, S.Y. Savrasov, *Phys. Rev. B* **83**, 205101 (2011).
- [15] M. Eto, K. Kasamatsu, M. Nitta, H. Takeuchi, M. Tsubota, *Phys. Rev. A* **83**, 063603 (2011).
- [16] E.Ö. Karabulut, F. Malet, A.L. Fetter, G.M. Kavoulakis, S.M. Reimann, *New J. Phys.* **18**, 015013 (2016).
- [17] R. Ravisankar, H. Fabrelli, A. Gammal, P. Muruganandam, P.K. Mishra, *Phys. Rev. A* **104**, 053315 (2021).
- [18] V. Achilleos, D.J. Frantzeskakis, P.G. Kevrekidis, D.E. Pelinovsky, *Phys. Rev. Lett.* **110**, 264101 (2013).
- [19] D. J. Frantzeskakis, *J. Phys. A* **43**, 213001 (2010).
- [20] L. Salasnich, W.B. Cardoso, B.A. Malomed, *Phys. Rev. A* **90**, 033629 (2014).
- [21] Z.G. Pu, J. Zhang, S. Yi, D.J. Wang, W.X. Zhang, *Phys. Rev. A* **93**, 053628 (2016).

- [22] K. Shirasawa, N. Kurita, H. Tanaka, *Phys. Rev. B* **96**, 144404 (2017).
- [23] N. Arakawa, *Phys. Rev. B* **99**, 014405 (2019).
- [24] T. Guo, J.N. Li, C.F. Mu, L.Y. He, *Phys. Rev. D* **106**, 094010 (2022).
- [25] J.H. Kim, D. Hong, S. Kang, Y. Shin, *Phys. Rev. A* **99**, 023606 (2019).
- [26] K. Tiurev, P. Kuopanportti, M. Möttönen, *Phys. Rev. A* **99**, 023621 (2019).
- [27] M. Tsubota, K. Kasamatsu, M. Ueda, *Phys. Rev. A* **65**, 023603 (2002).
- [28] R.K. Kumar, L.E. Young-S., D. Vudragović, A. Balaž, P. Muruganandam, S.K. Adhikari, *Comput. Phys. Commun.* **195**, 117 (2015).
- [29] P. Kaur, A. Roy, S. Gautam, *Comput. Phys. Commun.* **259**, 107671 (2021).
- [30] P. Banger, P. Kaur, A. Roy, S. Gautam, *Comput. Phys. Commun.* **279**, 108442 (2022).
- [31] E. Anderson, Z. Bai, C. Bischof, S. Blackford, J. Demmel, J. Dongarra, J. Du Croz, A. Greenbaum, S. Hammarling, A. McKenney, D. Sorensen, *LAPACK Users Guide*, SIAM, 1999.
- [32] Q. Zhao, H.J. Bi, X.M. Yang, L.L. Zhang, *Int. J. Mod. Phys. B* **36**, 2250050 (2022).
- [33] S. K. Adhikari, *J. Phys. Condens. Matter* **33**, 065404 (2021).
- [34] P. Banger, R.K. Kumar, A.S. Bradley, S. Gautam, *J. Phys. Condens. Matter* **35**, 045401 (2023).
- [35] S. Gautam, S.K. Adhikari, *Phys. Rev. A* **95**, 013608 (2017).
- [36] P. Kuopanportti, B.P. Anderson, M. Möttönen, *Phys. Rev. A* **87**, 033623 (2013).
- [37] S. Kang, J. Choi, S.W. Seo, W.J. Kwon, Y. Shin, *Phys. Rev. A* **91**, 013603 (2015).
- [38] T. Ollikainen, S. Masuda, M. Möttönen, M. Nakahara, *Phys. Rev. A* **95**, 013615 (2017).
- [39] J. Schloss, P. Barnett, R. Sachdeva, T. Busch, *Phys. Rev. A* **102**, 043325 (2020).
- [40] S. Sahar S. Hejazi, J. Polo, R. Sachdeva, T. Busch, *Phys. Rev. A* **102**, 053309 (2020).